Image Representations Using Multiscale Differential Operators

Yu-Ping Wang

***Abstract*— Differential operators have been widely used for multiscale geometric descriptions of images. The efficient computation of these differential operators is always desirable. Moreover, it has not been clear whether such representations are invertible. For certain applications, it is usually required that such representations should be invertible so that one can facilitate the processing of information in the transform domain and then recover it. In this paper, such problems are studied. We consider multiscale differential representations of images using different types of operators such as the directional derivative operators and Laplacian operators. In particular, we provide a general approach to represent images by their multiscale and multidirectional derivative components. For practical implementation, efficient pyramid-like algorithms are derived using spline technique for both the decomposition and reconstruction of images. It is shown that using these representations various meaningful geometric information of images can be extracted at multiple scales; therefore, these representations can be used for edge based image processing purposes. Furthermore, the intrinsic relationships of the proposed representations with the compact wavelet models, and some classical multiscale approaches are also elucidated in the paper.**

***Index Terms*— B-splines, computer vision, edge detection, image representation, scale-space, wavelet.**

I. Introduction

THE GEOMETRY of images is usually characterized using differential or difference operators such as the gradient operators, Laplacian operators and compass operators [29]. One of the most important geometric features of images is edges; they usually reflect the irregular structures and abrupt luminance changes of the image which are suitable for pattern recognition. However, it is well-known from both the psychophysical and physiological experiments that the edges of images are captured in the visual context of mammals at different resolution level. Therefore, the characterization of image features must be in a multiscale sense. Many researchers notably Burt and Adelson [1], Marr [3], Witkin [4], and Rosenfeld [38] have developed various scale-space approaches for multiscale information descriptions of images. As a new development of the classical scale-space theory, wavelets provide a more formal framework for multiscale representation [8], [11].

The general multiscale operation can be formulated using the following continuous wavelet transform:

$$Wf(s,t)=\int_{-\infty}^{\infty} f(x)\psi_s(t-x)\,dx, \quad s\in \mathbb{R}^+,\ t\in \mathbb{R} \tag{1}$$

where $\psi_s(x)=(1/s)\psi(x/s)$, $x\in\mathbb{R}$ is the scaled wavelet. In the classical scale-space theory, two frequently used operators are Marr–Hildreth operator [3] and Canny operator [5]. The wavelets are approximately the first and second derivatives of Gaussian. For two-dimensional (2-D) images, they are approximately the gradient operators of Gaussian and Laplacian of Gaussian (LoG). Edges are usually detected by examining either the local maxima or the zero-crossings of the resulting images convoluted with these two operators. Other image features such as the ridges, corners, blobs and junctions are also characterized by the local differential descriptors [17], [18]. In other applications such as the depth-from-stereo and optical flow, the gradient estimation is the first stage. The efficient computation of these differential operators is always desirable. Due to the high computational complexity of Gaussian kernel at large scales, there has been consistent interest in efficient computation of multiscale differential operators. For example, see Burt [1] and [2], Deriche [23], Wells [24], and Ferrari *et al.* [25]. Also, it has not been clear whether images can be recovered from these multiscale differential components. For some applications it usually requires that such representations are invertible so that one can facilitate the processing of information in the transform domain and then recover it.

In this paper, we aim at providing efficient algorithms for multiscale computation and representation of images using differential operators starting with the standard B-spline theory. Because B-splines provide stable and hierarchical representations [22] and have other good properties [13], we use B-splines to first parameterize the image surface and then compute the differential operations. These differential operators include the directional derivative operators, Laplacian operators and multidirectional derivative operators. Similar to the wavelets design, we also derive pyramid-like filter bank algorithms for the decomposition and synthesis of images using these differential operators. Different from the compact wavelets models [8], the derived representations are *shift-invariant* and have explicit physical meaning which are very suitable for geometry based image processing.

Manuscript received April 15, 1998; revised March 23, 1999. This work was supported by the Wavelets Strategic Research Programme funded by the National Science and Technology Board and Ministry of Education of Singapore under Grant RP960 601/A. The associate editor coordinating the review of this manuscript and approving it for publication was Dr. Fabrice Heitz.

The author was with the Wavelets Strategic Research Programme, National University of Singapore, Republic of Singapore 119260. He is now with Washington University Medical School, St. Louis, MO 63130 USA (e-mail: wyp@cauchy.wustl.edu).

Publisher Item Identifier S 1057-7149(99)09352-5.

The rest of the paper is organized as follows. In Section II, we provide basic multiscale spline approximation theory and discuss the comparison of B-splines with the classical scale-space kernels. In Section III, 1-D signal representations using the first and second order derivatives or differences are considered. Both the recursive and parallel algorithms are investigated. All the filters for the discrete implementations of decomposition and reconstruction are given explicitly as binomials which only need *addition* operation. Extensions to 2-D images are given in Section IV, where the representations of the images using multiscale second directional derivative operators and Laplacian operators are considered in detail. In the following section, a general procedure is presented to decompose and reconstruct images from their multiscale and multidirectional derivative components. Finally, some discussions and conclusions are given.

II. Multiresolution Polynomial Spline Function Approximation of $L^2(\mathbb{R})$

A. Multiresolution Spline Function Approximation of $L^2(\mathbb{R})$

Suppose $L^2(\mathbb{R})$ is the Hilbert space of finite energy functions and $l^2(\mathbb{Z})$ is the space of finite energy discrete sequences. Let $h > 0$ and define the polynomial spline space S_h^n consisting of the dilated and shifted B-splines of order n (n is assumed to be odd throughout the paper) by

$$S_h^n = \left\{ \sum_{k=-\infty}^{+\infty} c_h(k)\beta_h^n(x - hk) : c_h \in l^2(\mathbb{Z}) \right\} \tag{2}$$

where $\beta_h^n(x) = (1/h)\beta^n(x/h)$. $\beta^n(x)$ is defined as the central *continuous B-spline of order n*, which can be generated by $n+1$-fold convolution of the B-spline of order 0

$$\beta^n(x) = \beta^0 * \beta^{n-1}(x) = \overbrace{\beta^0 * \beta^0 * \cdots * \beta^0(x)}^{n+1}, \quad x \in \mathbb{R} \tag{3}$$

where the zeroth-order B-spline $\beta^0(x)$ is the unit pulse function with the support $[(-1/2), 1/2]$. It is easy to show that the Fourier transform of $\beta^n(x)$ is

$$\begin{aligned} \hat{\beta}^n(\omega) &= \left[\hat{\beta}^0(\omega)\right]^{n+1} \\ &= \left(\frac{\sin\frac{\omega}{2}}{\frac{\omega}{2}}\right)^{n+1} \\ &= \operatorname{sinc}^{n+1}\frac{\omega}{2}, \quad \omega \in \mathbb{R}. \end{aligned} \tag{4}$$

It can be shown that the B-spline spaces constitute a multiresolution of $L^2(\mathbb{R})$ [22]:

$$S_{mh}^n \subset S_h^n, \quad \forall\, m \in \mathbb{Z}^+, \tag{5}$$

$$\overline{\bigcup_{h>0} S_h^n} = L^2(\mathbb{R}). \tag{6}$$

The embedding property (5) follows from the fact that B-splines are m-refinable, i.e., it should satisfy the following m-scale relation:

$$\frac{1}{m}\beta^n\left(\frac{x}{m}\right) = \sum_{k=-\infty}^{+\infty} B_m^n(k)\beta^n(x-k), \quad x \in \mathbb{R} \tag{7}$$

where

$$B_m^n = \overbrace{B_m^0 * B_m^0 * \cdots B_m^0}^{n+1}$$

is *the discrete B-spline of order n at scale m* and $B_m^0 = (1/m)[1, 1, \cdots, 1]$ is a normalized sampled pulse of width m. The m-refinability of the B-splines indicated in (7) can be easily verified [22].

Property (6) indicates that any signal $f \in L^2(\mathbb{R})$ can be projected as a weighted sum of translated and dilated B-splines in the certain resolution space (suppose one for simplicity) S_1^n

$$f(x) = \sum_{k=-\infty}^{+\infty} c_k\beta^n(x-k), \quad x \in \mathbb{R} \tag{8}$$

and the coefficients $c_k \in l^2(\mathbb{Z})$ can be computed efficiently [16]. Moreover, as proved in [22], the shifted B-splines are the only spline bases which are m-refinable and constitute Riesz bases, i.e.,

$$A\|f\|^2 \le \sum_{k=-\infty}^{+\infty} |c_k|^2 \le B\|f\|^2, \quad \text{with } A, B > 0. \tag{9}$$

Therefore, this energy equivalence guarantees that such an approximation is also numerically stable. Different resolution levels imply different effects of smoothing. The larger is the value of scale m, the better the smoothing effect of the signal or less influence of the noise. But, conversely the less accurate is the edge localization.

If we restrict the scales to be dyadic, from (5) the following simple relation can be derived:

$$S_{2^{m+1}}^n \subset S_{2^m}^n, \quad m \in \mathbb{Z}. \tag{10}$$

From the fact that the spline function spaces $S_{2^m}^n$ are nested we know that the basis functions at the coarser levels are themselves included in the finer resolution spaces. In particular, we have the following two-scale relation:

$$\frac{1}{2}\beta^n\left(\frac{x}{2}\right) = \sum_{k=-\infty}^{+\infty} h_k\beta^n(x-k), \quad x \in \mathbb{R} \tag{11}$$

or equivalently in the Fourier domain

$$\hat{\beta}^n(2\omega) = H(\omega)\hat{\beta}^n(\omega), \quad \omega \in \mathbb{R} \tag{12}$$

where

$$H(\omega) = \sum_{k=-\infty}^{+\infty} h_k e^{i\omega} = \left(\cos\frac{\omega}{2}\right)^{n+1}. \tag{13}$$

It is easy to infer through the binomial expansion that the corresponding finite impulse responses (FIR's) are

$$h_k = \begin{cases} \dfrac{1}{2^{n+1}}\binom{n+1}{\frac{n+1}{2}+k}, & \text{if } |k| \le n+1 \\ 0, & \text{elsewhere} \end{cases} \tag{14}$$

where $\binom{n}{k} = [n!/k!(n-k)!]$ is the binomial coefficient.

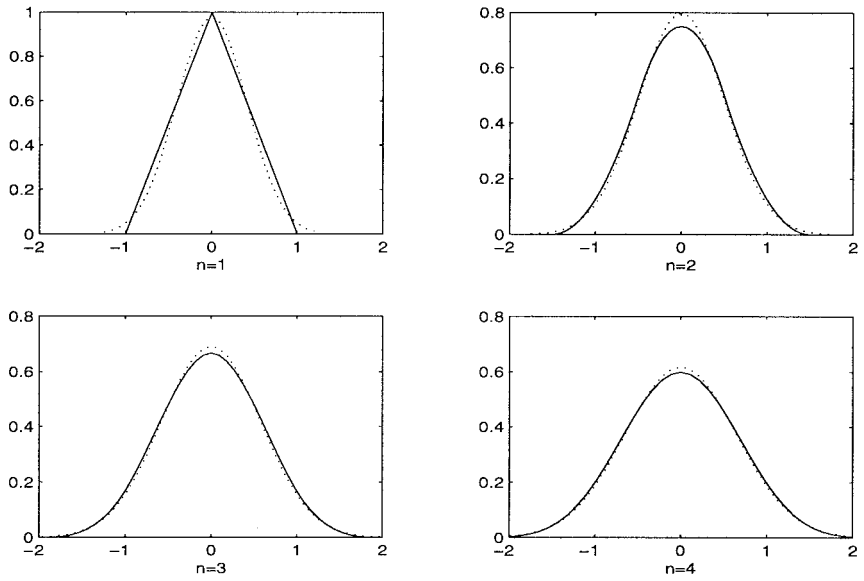

Fig. 1. Comparison of the lower order B-splines (in solid line) with the Gaussian function (in dotted line). They have the approximate relation $\beta^n(x) \approx \sqrt{6/\pi(n+1)}\,\exp(-(6x^2/n+1))$. Higher order of B-splines, closer approximations to Gaussian.

It can be shown easily that in the discrete setting the above conclusion also holds in $l^2(\mathbb{Z})$ if we take the spatial variable x as integer [15].

B. Comparison with Some Scale-Space Kernels

As shown above, one of the prominent properties of B-splines is that they can provide stable and hierarchical representation of a signal at different scales. For other advantages of B-spline technique, refer to [13]. In particular, B-splines are good approximations to the Gaussian kernel which is commonly used in computer vision. A more rigorous proof as well as the numerical evidence underlining the uncertainty principle was given in [14], which showed that both B-splines and their Fourier transforms converge to the Gaussian function in $L^p(\mathbb{R})$, $p \in \mathbb{Z}^+$ as the order of the spline n tends to infinity. This is illustrated in Fig. 1. Although Gaussian is regarded as the only kernel that has the scaling property for multiscale representation [36], [37], from the regularity theory, the cubic B-spline is regarded as optimal for edge detection [12]. The comparison of B-spline filters with Gaussian and other famous filter windows can be found in [19].

It is quite interesting in the formulation of discrete scale-space theory [18], the Gaussian kernel was discretized in the spatial domain and approximated by a family of kernels $T(n; s) = \exp(-s)I_n(s)$, where $I_n(s)$ are the modified Bessel functions of integer order and s indexes the continuous scale. The discrete B-spline or binomial filters and these kernels can be classified in terms of total positivity theory. All shift invariant discrete scale-space kernels are equivalent to normalized pólya frequencies and the discrete scale-space kernels of finite support arise from generalized binomial smoothing. The one-dimensional (1-D) B-spline filters should be a specialized class of transition operators in discrete linear scale-space theory [18]. Like these discrete kernels in [18], B-splines are used for computational efficiency as will be discussed in the following sections.

III. 1-D Signal Representation by its Multiscale Differential Operators

We begin with the 1-D case. We have the signal approximation (8) at the finest scale space S_1^n, and want to analyze the geometric information in the coarser scale space $\{S_{2^j}^n\}_{j\in\mathbb{Z}}$. For this purpose, the following wavelets are defined.

A. The Choices of Spline Wavelets

Since the geometrical features are characterized by the differential operators, the wavelets in (1) are usually taken as the kth-order derivatives of a smooth function. Equivalently, the wavelets are required to satisfy the following vanishing moments condition:

$$\int_{-\infty}^{\infty} x^{k-1}\psi(x)\,dx = 0, \quad k \in \mathbb{Z}. \tag{15}$$

Since B-splines constitute stable bases of $L^2(\mathbb{R})$ or $l^2(\mathbb{Z})$, we use the B-splines to approximate or represent the wavelets too. The advantage of this approach is due to the computational efficiency and the fast computation of the continuous wavelet transform (1) or scale-space filtering at any rational scales can be obtained [20].

We give some typical choices of the spline wavelets.

- *Canny Operator-Like Wavelets:* Because of the close approximations of B-splines to Gaussian, we choose the B-spline wavelets to be the first derivative or difference of B-splines which are similar to the Canny operator [5]. The B-spline wavelets of order n are taken as the first derivatives of B-splines of order $n+1$ at the resolution 2^{-1}.

$$\begin{aligned}\psi^n(x) &= \frac{1}{2}\frac{d}{dx}\beta_{2^{-1}}^{n+1}(x)\\ &= 2\left(\beta^n\left(2x+\frac{1}{2}\right) - \beta^n\left(2x-\frac{1}{2}\right)\right),\\ &\qquad x \in \mathbb{R}\end{aligned} \tag{16}$$

which are also the first-order of differences of B-splines of order n at the resolution 2^{-1} [20]. Equivalently, in the Fourier domain, they can be written as

$$\hat{\psi}^n(\omega) = \frac{i\omega}{2}\,\hat{\beta}^{n+1}\Big(\frac{\omega}{2}\Big) = 2i\,\sin\frac{\omega}{4}\,\hat{\beta}^n\Big(\frac{\omega}{2}\Big), \quad \omega \in \mathbb{R}. \tag{17}$$

- *LoG-Like Wavelets:* Similarly, if we take the wavelets as the second order derivatives of B-splines, we will obtain the LoG-like or Mexican hat like wavelets [3]. In detail, the wavelets are given as

$$\psi^n(x) = \frac{1}{4}\frac{d^2}{dx^2}\beta^{n+2}_{2^{-1}}(x) = 2(\beta^n(2x+1) - 2\beta^n(2x) + \beta^n(2x-1)), \quad x \in \mathbb{R} \tag{18}$$

or equivalently in the Fourier domain

$$\hat{\psi}^n(\omega) = -\frac{1}{4}(i\omega)^2\hat{\beta}^{n+2}\Big(\frac{\omega}{2}\Big) = \Big(2i\,\sin\frac{\omega}{4}\Big)^2\hat{\beta}^{n+2}\Big(\frac{\omega}{2}\Big), \quad \omega \in \mathbb{R} \tag{19}$$

which are also the second order differences of B-splines of order n at the resolution level 2^{-1}.

- *DoG-Like Wavelets:* If we take the spline wavelets as the difference of B-splines at the adjacent resolutions, we obtain the DoG-like wavelets [7]:

$$\psi^n(x) = 2\beta^n(2x) - \beta^n(x), \quad x \in \mathbb{R}. \tag{20}$$

Since B-splines are good approximations to Gaussian, the wavelets selected above are good approximations to some famous classical operators [3], [5], [7]. It is easy to verify that these wavelets have one and two vanishing moments. Different order of vanishing moments can detect edges with different singularities [10].

The graphs of the first two spline wavelets of order $n = 3$ are shown in Fig. 2. They are symmetric and antisymmetric, respectively.

B. Fast Recursive Algorithms for the Decomposition and Reconstruction

When selecting the wavelets as in (16), (18), and (20) one can extract the geometric information at coarser scale approximation $\{S^n_{2^j}\}_{1\le j\le J}$ from the finest scale approximation S^n_1. Through the refinable properties of the B-splines (7), fast algorithm at rational scales was achieved [20]. Here we restrict to the dyadic scales $\{2^j\}_{j\in\mathbb{Z}}$ to obtain more compact multiscale representations of signals, which are called the *dyadic wavelet transforms.*

First, it can be shown that our selected wavelets (16) and (18) satisfy the following two-scale relations with the scaling function of B-splines:

$$\frac{1}{2}\,\psi^n\Big(\frac{x}{2}\Big) = \sum_{k=-\infty}^{\infty} g_k\beta^n(x-k), \quad x \in \mathbb{R} \tag{21}$$

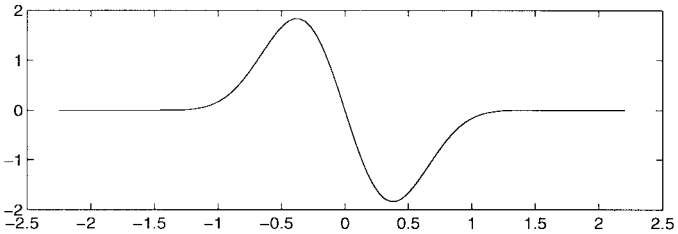

(a)

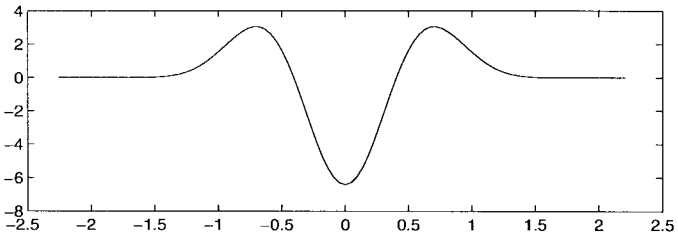

(a)

Fig. 2. Cubic B-spline wavelets: (a) Canny operator-like wavelets and (b) LoG-like wavelets.

or in the Frequency domain

$$\hat{\psi}^n(2\omega) = G(\omega)\hat{\beta}^n(\omega), \quad G(\omega) = \sum_{k=-\infty}^{\infty} g_k e^{-ik\omega}. \tag{22}$$

If the wavelets are taken as (16) and (18), we can obtain the explicit expressions of the transfer function G and the corresponding FIR's in the time domain.

- If the wavelets ψ^n are taken as (16), then $G(\omega) = 2i\,\sin(\omega/2)$ and the corresponding FIR's are

$$g_0 = -1, \quad g_1 = 1, \quad g_k = 0 \quad (k \neq 0, 1) \tag{23}$$

which is the first-order difference operator, modulo a shift $\delta(x - (1/2))$.

- If ψ^n are chosen as (18), then $G(\omega) = -4\,\sin^2(\omega/2)$ and the corresponding FIR's are

$$g_{-1} = 1, \quad g_0 = -2, \quad g_1 = 1, \quad g_k = 0 \quad (k \neq -1, 0, 1) \tag{24}$$

which is the second-order difference operator.

If the following smoothing operations $\{S_{2^j}f\}_{j\in\mathbb{Z}}$ and wavelet transforms $\{W_{2^j}f\}_{j\in\mathbb{Z}}$ are introduced:

$$S_{2^j}f = f * \beta^n_{2^j}, \quad W_{2^j}f = f * \psi^n_{2^j}, \quad j = 1, 2, \cdots, J \tag{25}$$

one can see that the wavelet transforms $\{W_{2^j}f\}_{j\in\mathbb{Z}}$ are just the first and second derivatives of the signal $f \in L^2(\mathbb{R})$ smoothed by the B-splines along the resolutions $\{2^j\}_{j\in\mathbb{Z}}$. By the two-scale relation (11), (21), the following recursive algorithm can be obtained

$$\begin{cases} S_{2^j}f[n] = \sum_{k\in\mathbb{Z}} h_k S_{2^{j-1}}f[n - 2^{j-1}k] \\ W_{2^j}f[n] = \sum_{k\in\mathbb{Z}} g_k S_{2^{j-1}}f[n - 2^{j-1}k], \\ \qquad j = 1, 2, \cdots, J. \end{cases} \tag{26}$$

In addition, if we define the *upsampling* operation of a sequence $h(n)$ by an integer multiple m as $[h]_{\uparrow m}$, then the above decomposition formula can be simply written as

$$\begin{cases} S_{2^j} f = S_{2^{j-1}} f * h_{\uparrow 2^{j-1}} \\ W_{2^j} f = S_{2^{j-1}} f * g_{\uparrow 2^{j-1}}, \qquad j = 1, 2, \cdots, J. \end{cases} \tag{27}$$

This algorithm can be called the *pyramid-like algorithm*. In comparison with the standard wavelets pyramid algorithm [8], at each scale decomposition no down-sampling is done. $S_{2^0} f$ is usually taken as the original sampled signal $\{f(n)\}_{1 \le n \le N}$. Or more accurately, it can be computed using the efficient algorithm proposed in [16]. The complexity of the recursive algorithm (26) or (27) is $\mathcal{O}(N \log_2 N)$.

In order to make the above decomposition procedure to be invertible, we design the reconstruction filters $\tilde{H}$ and $\tilde{G}$ to satisfy the following perfect reconstruction condition [8], [11]

$$\forall\, \omega \in \mathbb{R} \quad H(2^{j-1}\omega)\tilde{H}(2^{j-1}\omega) + G(2^{j-1}\omega)\tilde{G}(2^{j-1}\omega) = 1. \tag{28}$$

For simplicity, we just take the synthesis filter $\tilde{H}$ as $\overline{H}$ ($\tilde{h} = \overline{h}$). Then through (28) we can derive the explicit expression of $\tilde{G}$ and the corresponding FIR's.

- If ψ is taken as (16), then by (13) and (23)

$$\tilde{G}(\omega) = \frac{1 - \cos^{2n+2}\frac{\omega}{2}}{2i \sin\frac{\omega}{2}} = \frac{1}{2i} \sin\frac{\omega}{2} \sum_{j=0}^{n} \left(\cos^2\frac{\omega}{2}\right)^j \tag{29}$$

  and the corresponding FIR's are shown in (30), at the bottom of the page.

- If ψ is defined as (18), then by (13) and (24)

$$\tilde{G}(\omega) = \frac{1 - \cos^{2n+2}\frac{\omega}{2}}{-4\sin^2\frac{\omega}{2}} = -\frac{1}{4} \sum_{j=0}^{n} \left(\cos^2\frac{\omega}{2}\right)^2 \tag{31}$$

  and the corresponding FIR's are

$$\tilde{g}_l = \begin{cases} -\frac{1}{4} \sum_{j=|l|}^{j=n} \frac{1}{2^{2j}} \binom{2j}{j+|l|} & |l| \le n \\ 0 & \text{otherwise.} \end{cases} \tag{32}$$

Through (11) and (21) and the inverse Fourier transform of the reconstruction condition (28), one can reconstruct signal $S_1 f$ from its dyadic wavelet transforms $\{W_{2^j}\}_{1 \le j \le J} \bigcup S_{2^J} f$ using the following formula

$$S_{2^{j-1}} f[n] = \sum_{k \in \mathbb{Z}} (h_k S_{2^j} f[n - 2^{j-1}k] + \tilde{g}_k W_{2^j} f[n - 2^{j-1}k]), \quad n \in \mathbb{Z} \tag{33}$$

or simply written as

$$S_{2^{j-1}} f = S_{2^j} f * h_{\uparrow 2^{j-1}} + W_{2^j} f * \tilde{g}_{\uparrow 2^{j-1}}. \tag{34}$$

Furthermore, if we define the reconstructing filter χ^n by

$$\hat{\chi}^n(2\omega) = \tilde{G}(\omega)\hat{\beta}^n(\omega), \qquad \omega \in \mathbb{R} \tag{35}$$

it is easy to show through (28) that the signal $f \in L^2(\mathbb{R})$ can be reconstructed from its dyadic wavelet transforms or derivative components $\{W_{2^j} f\}_{j \in \mathbb{Z}}$ in the continuous form as

$$f(x) = \sum_{j=-\infty}^{+\infty} W_{2^j} f * \chi_{2^j}^n(x), \qquad x \in \mathbb{R}. \tag{36}$$

The dyadic wavelet transforms of a simulated signal consisting of different types of edges using the cubic wavelets are illustrated in Fig. 3. The behaviors of the edges across several scales are displayed.

If the wavelets are taken as (20), the corresponding wavelet decompositions are just the differences of two different smoothing operations

$$W_{2^j} f[n] = S_{2^{j-1}} f[n] - S_{2^j} f[n], \quad n \in \mathbb{Z}$$

and the reconstruction formula reads

$$S_{2^{j-1}} f[n] = W_{2^j} f[n] + S_{2^j} f[n], \quad n \in \mathbb{Z}.$$

In [6] a family of recursive filters are proposed, which is optimized according to the criteria similar to Canny [5]. Hence, they are more suitable for edge detection applications. But a little bit more computational costs are needed than ours. Moreover, the reconstruction system that these filters satisfy is more strict than ours as in (28). For our design G and $\tilde{G}$ are not required to be a quadrature pair in (28).

$$\tilde{g}_l = \begin{cases} \frac{1}{2^{2n+2}}, & l = -(n+1) \\ -\sum_{j=-l}^{n} \frac{1}{2^{2j+2}} \binom{2j}{j+l} + \sum_{j=-l}^{n+1} \frac{1}{2^{2j}} \binom{2(j-1)}{j+l}, & -n \le l \le -1 \\ -\sum_{j=l}^{n} \frac{1}{2^{2j+2}} \binom{2j}{j+l} + \sum_{j=l}^{n+1} \frac{1}{2^{2j+4}} \binom{2(j+1)}{j+l+2}, & 0 \le l \le n-1 \\ -\frac{1}{2^{2n+2}} & l = n \\ 0, & \text{otherwise} \end{cases} \tag{30}$$

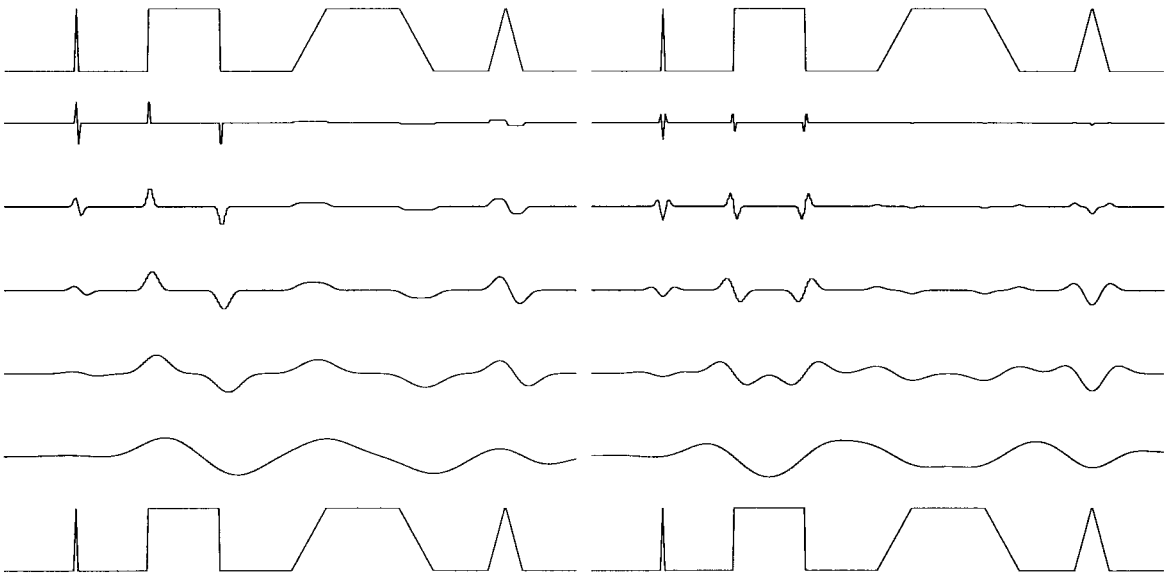

Fig. 3. Dyadic spline wavelet decomposition and reconstruction of a simulated signal containing different types of edges. At the top row is the simulated signal, at the bottom row is the reconstructed signal. Left: using the Canny operator-like wavelets. Right: using the LoG-like wavelets.

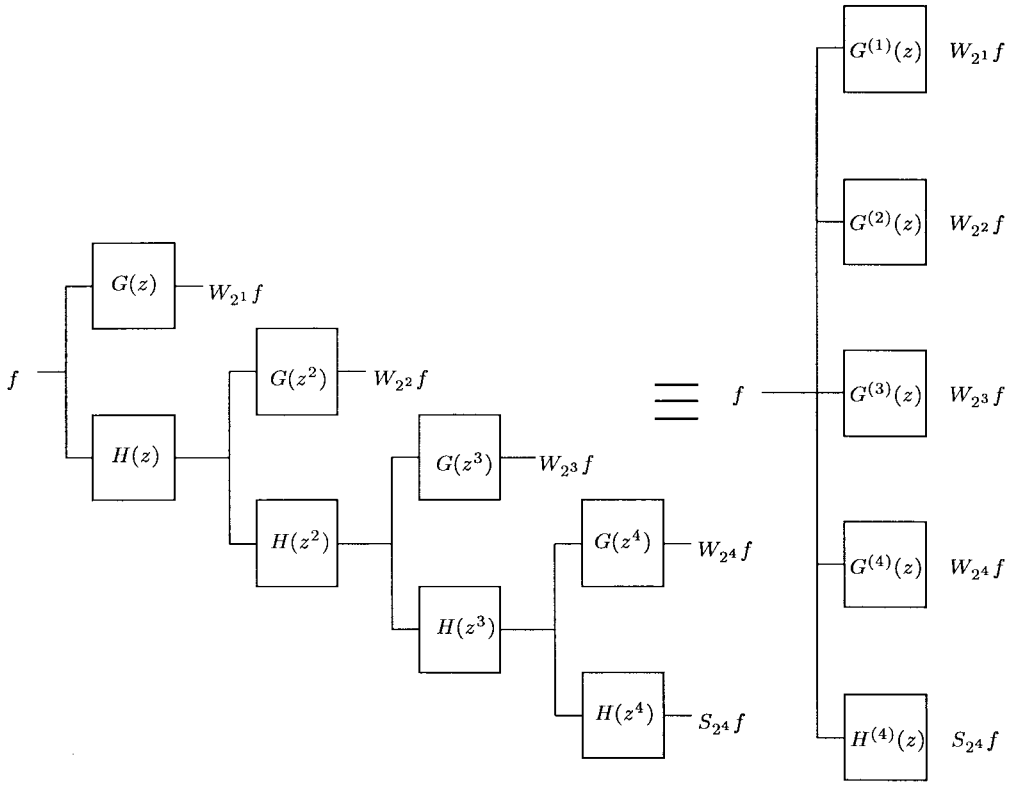

Fig. 4. Parallel realization of the algorithm. Every filter in the diagram can be realized only by *addition* and *bit shift* operation.

C. Parallel Implementation and Improvement of Computational Speed

One can have a parallel implementation of the dyadic wavelet transforms without resorting to the recursive pyramid-like algorithms (26) and (33). This is illustrated in Fig. 4. The intrinsic relations between the filter banks, binomial and the spline wavelets are discussed in Appendix A.

The smooth approximations $\{S_{2^j}\}_{1\le j\le J}$ and the wavelet transforms $\{W_{2^j}\}_{1\le j\le J}$ along different scales can be computed simultaneously and directly from the finest scale approximation $S_{2^0}f$ using the following formula:

$$\begin{cases} S_{2^j}f = S_{2^0}f * h^{(j)}, \\ W_{2^j}f = S_{2^0}f * g^{(j)}, \qquad j = 1, 2, \cdots, J. \end{cases} \tag{37}$$

The binomial filter $h^{(j)}$ can be obtained easily from the following iterative relation:

$$h^{(j)}[n] = \frac{1}{2^{n+1}} \sum_{l=0}^{n+1} \binom{n+1}{k} h^{(j-1)}[n - 2^{j-1}l], \quad n \in \mathbb{Z} \tag{38}$$

and $g^{(j)}$ is obtained by taking the first- or second-order difference of the sequence $h^{(j)}$ with a spacing 2^{j-1}. The frequency responses of these filters are given as (74) and (75) in Appendix A.

In the meantime, since all the filters $h^{(j)}$, $g^{(j)}$ are linear combinations of binomials, the computational efficiency can be further improved using the *Pascal triangular algorithm*. In detail, due to the following identity:

$$\binom{n}{k} = \binom{n-1}{k} + \binom{n-1}{k-1}$$

the convolution with a nth binomial can be realized using only *addition* operation recursively from zeroth binomial (unit impulse). The last normalization factor $1/2^{n+1}$ can be implemented directly by the operation of *bit shift* rather than multiplication. We can call this method as the *moving average sum technology*, which lead to an easy hardware realization. The complexity of approach is $\mathcal{O}(N)$ and hence an improvement over the recursive algorithms (26) and (33) with the complexity $\mathcal{O}(N \log_2 N)$.

IV. Extension to 2-D Images

A. Decomposition and Reconstruction of an Image from Its Directional Derivative Components

The above results for 1-D signal can be easily extended to the 2-D case. By tensor product, the 2-D smoothing function is taken as $\beta^n(x, y) = \beta^n(x)\beta^n(y) \in L^2(\mathbb{R}^2)$. Now we show how images can be decomposed and reconstructed from its multiscale differential components via spline technique. As an example, the second directional derivative case is considered. The gradient operator case was discussed in [9] and in fact can be further refined using spline technique.

A usual approach for edge detection is to detect the zero-crossings of the second directional derivative of the smoothed image $f * \beta^n_{2^j}(x, y)$ along the gradient orientation

$$\begin{aligned}\frac{\partial^2 (f * \beta^n_{2^j}(x,y))}{\partial n^2} &= \frac{\partial^2 (f * \beta^n_{2^j}(x,y))}{\partial x^2} \cos^2\theta + 2\frac{\partial^2 (f * \beta^n_{2^j}(x,y))}{\partial x \partial y} \\ &\quad \cdot \cos\theta \sin\theta + \frac{\partial^2 (f * \beta^n_{2^j}(x,y))}{\partial y^2} \sin^2\theta. \end{aligned} \tag{39}$$

We can also use the recursive procedure to compute the three directional derivative components or wavelet transforms

$$W^1_{2^j} f(x, y) = \frac{\partial^2 (f * \beta^n_{2^j}(x,y))}{\partial x^2}, \tag{40}$$

$$W^2_{2^j} f(x, y) = \frac{\partial^2 (f * \beta^n_{2^j}(x,y))}{\partial y^2}, \tag{41}$$

$$W^3_{2^j} f(x, y) = \frac{\partial^2 (f * \beta^n_{2^j}(x,y))}{\partial x \partial y} \tag{42}$$

where the three directional wavelets are defined as

$$\begin{aligned}\hat{\psi}^{n,1}(2\omega_x, 2\omega_y) &= G^{(2)}(\omega_x)\hat{\beta}^n(\omega_x, \omega_y), \\ \hat{\psi}^{n,2}(2\omega_x, 2\omega_y) &= G^{(2)}(\omega_y)\hat{\beta}^n(\omega_x, \omega_y), \\ \hat{\psi}^{n,3}(2\omega_x, 2\omega_y) &= G^{(1)}(\omega_x)G^{(1)}(\omega_y)\hat{\beta}^n(\omega_x, \omega_y). \end{aligned} \tag{43}$$

For clarity, here we denote $G^{(1)}$ and $G^{(2)}$ the transfer functions of the first and second order of difference operators $g^{(1)}$, $g^{(2)}$ given by (23) and (24). Then, from these definitions we can obtain a recursive algorithm for the computation of these three local partial derivative components along the dyadic sequences $\{2^j\}_{j\in\mathbb{Z}}$:

$$\begin{cases} S_{2^j} f = S_{2^{j-1}} f * (h, h)_{\uparrow 2^{j-1}} \\ W^1_{2^j} f = S_{2^{j-1}} f * (g^{(2)}, d)_{\uparrow 2^{j-1}} \\ W^2_{2^j} f = S_{2^{j-1}} f * (d, g^{(2)})_{\uparrow 2^{j-1}} \\ W^3_{2^j} f = S_{2^{j-1}} f * (g^{(1)}, g^{(1)})_{\uparrow 2^{j-1}} \end{cases} \tag{44}$$

where $I * (h, g)_{\uparrow 2^{j-1}}$ represents the separable convolution of the rows and columns of the image with the 1-D filters $[h]_{\uparrow 2^{j-1}}$ and $[g]_{\uparrow 2^{j-1}}$, respectively. The symbol d denotes the Dirac filter whose impulse is one at the origin and zero elsewhere.

In order to obtain the reconstruct formula, we design the following perfect reconstruction condition:

$$\begin{aligned} H^2(\omega_x)H^2(\omega_y) &+ G^{(2)}(\omega_x)\tilde{G}^{(2)}(\omega_x)U(\omega_y) \\ &+ G^{(2)}(\omega_y)\tilde{G}^{(2)}(\omega_y)U(\omega_x) \\ &+ G^{(1)}(\omega_x)\tilde{G}^{(1)}(\omega_x)G^{(1)}(\omega_y)\tilde{G}^{(1)}(\omega_y) = 1 \end{aligned} \tag{45}$$

where $\tilde{G}^{(1)}$, $\tilde{G}^{(2)}$ correspond to $G^{(1)}$, $G^{(2)}$ and satisfy the perfect reconstruction condition specified by (28). $U(\omega) = H^2(\omega)$.

Using this condition it is easy to obtain the following discrete reconstruction formula:

$$\begin{aligned} S_{2^{j-1}} f = W^1_{2^j} f * (\tilde{g}^{(2)}, u)_{\uparrow 2^{j-1}} &+ W^2_{2^j} f * (u, \tilde{g}^{(2)})_{\uparrow 2^{j-1}} \\ &+ W^3_{2^j} f * (\tilde{g}^{(1)}, \tilde{g}^{(1)})_{\uparrow 2^{j-1}} + S_{2^j} f * (h, h)_{\uparrow 2^{j-1}} \end{aligned} \tag{46}$$

where $u(j) = 1/2^{2n+2}\binom{2n+2}{j}$, $0 \le j \le 2n+2$, are the FIR's of the transfer function $U(\omega) = H^2(\omega)$, $\tilde{g}^{(1)}$ and $\tilde{g}^{(2)}$ are impulse responses of $\tilde{G}^{(1)}$ and $\tilde{G}^{(2)}$.

Furthermore, if we define the three corresponding reconstruction wavelets as

$$\begin{aligned} \hat{\chi}^{n,1}(\omega_x, \omega_y) &= \tilde{G}^{(2)}(\omega_x)H^2(\omega_y)\hat{\beta}^n(\omega_x, \omega_y), \\ \hat{\chi}^{n,2}(\omega_x, \omega_y) &= \tilde{G}^{(2)}(\omega_y)H^2(\omega_x)\hat{\beta}^n(\omega_x, \omega_y), \\ \hat{\chi}^{n,3}(\omega_x, \omega_y) &= \tilde{G}^{(1)}(\omega_x)\tilde{G}^{(1)}(\omega_y)\hat{\beta}^n(\omega_x, \omega_y) \end{aligned} \tag{47}$$

then the image $f(x, y) \in L^2(\mathbb{R}^2)$ can be recovered from the three directional derivative components $\{W^k_{2^j}\}^{k=1,2,3}_{j\in\mathbb{Z}}$ in the continuous form as

$$\begin{aligned} f(x, y) = \sum_{j=-\infty}^{\infty} \big(&W^1_{2^j} f * \chi^{n,1}(x, y) + W^2_{2^j} f * \chi^{n,2}(x, y) \\ &+ W^3_{2^j} f * \chi^{n,3}(x, y) \big), \quad (x, y) \in \mathbb{R}^2. \end{aligned} \tag{48}$$

Fig. 5 illustrates this algorithm procedure. The dyadic decomposition and reconstruction of a simulated image using three directional derivative components are displayed. Since all the filters in the decomposition and reconstruction formulae are binomials, only addition is needed.

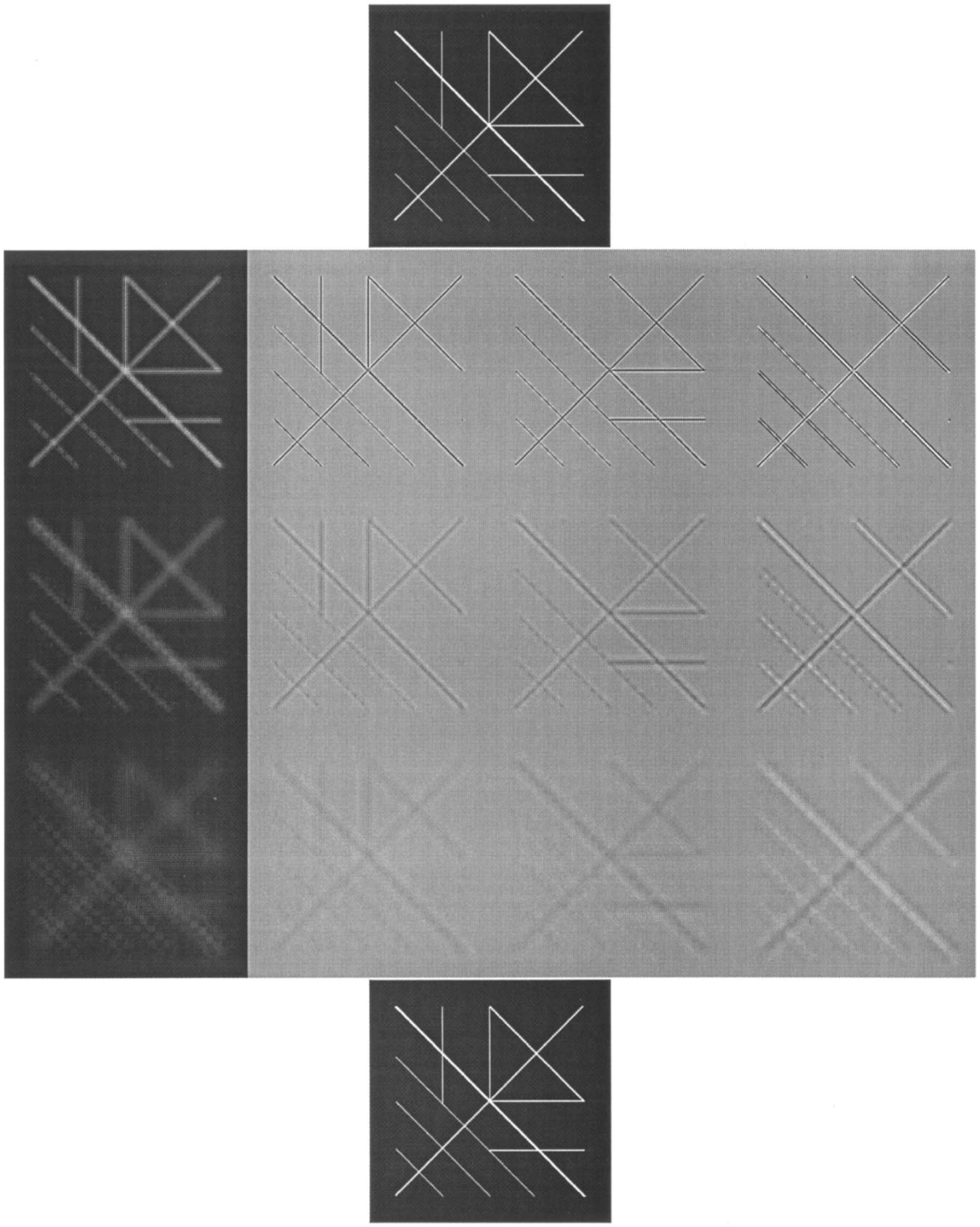

Fig. 5. Representation of a simulated 512 × 512 image by its second-order of directional derivative components at dyadic scales. The order of B-splines used is four. At the top row is the simulated square image and at the bottom row is the reconstructed image. Between them are the smoothing part and the directional decompositions along the horizontal, vertical, and diagonal orientations at dyadic scales 1, 2, and 4, respectively. Using spline technique, the decomposition and reconstruction can be efficiently computed using only additions.

B. Decomposition and Reconstruction of Images from Multiscale LoG-Like Components

Another widely used differential operator is the Laplacian operator:

$$\nabla^2 f(x, y) = \left(\frac{\partial^2}{\partial x^2} + \frac{\partial^2}{\partial y^2} \right) f(x, y) \tag{49}$$

which is isotropic with respect to the orientation. Torre and Poggio [12] have carried an extensive investigation on the relationship between the Laplacian and the second directional operators. In practice, the Laplacian of Gaussian (LoG) operator is widely used for multiscale image analysis [3]. In this section we attempt to find similar filter bank algorithms to

decompose and reconstruct images using multiscale LoG-like components.

Our starting point is to consider the multiresolution approximation on the circle. The perfect reconstruction condition (28) in 1-D case are extended to the 2-D polar coordinate case as

$$H^2(\omega_x, \omega_y) + G(\omega_x, \omega_y)\tilde{G}(\omega_x, \omega_y) = 1 \tag{50}$$

and the decomposition and reconstruction filters H, G, $\tilde{G}$ are given by

$$\begin{aligned} H(\omega_x, \omega_y) &= H(r) = \left(\cos\frac{r}{2}\right)^{n+1}, \\ G(\omega_x, \omega_y) &= G(r) = -4\sin^2\frac{r}{2}, \end{aligned} \tag{51}$$

$$\tilde{G}(\omega_x, \omega_y) = H(r) = -\frac{1}{4}\sum_{j=0}^{n}\left(\cos\frac{r}{2}\right)^j, \tag{52}$$

where the radius

$$r = \min\left(\sqrt{\omega_x^2 + \omega_y^2}, \pi\right), \quad -\pi \le \omega_x, \omega_y \le \pi$$

is taken such that these filters are defined in a finite domain.

The 2-D nonseparable scaling or smoothing function is defined by

$$\hat{\varphi}^n(\omega_x, \omega_y) = \mathrm{sinc}^{n+1}\left(\tfrac{1}{2}\sqrt{\omega_x^2 + \omega_y^2}\right) \tag{53}$$

which is the *radial B-spline of order n*. The isotropic wavelet function and the reconstruction wavelets are defined by

$$\begin{aligned} \hat{\psi}^n(2\omega_x, 2\omega_y) &= -(\omega_x^2 + \omega_y^2)\hat{\varphi}^{n+2}(\omega_x, \omega_y) \\ &= G(\omega_x, \omega_y)\hat{\varphi}^n(\omega_x, \omega_y), \end{aligned} \tag{54}$$

$$\hat{\chi}^n(2\omega_x, 2\omega_y) = \tilde{G}(\omega_x, \omega_y)\hat{\varphi}^n(\omega_x, \omega_y). \tag{55}$$

The impulse responses of these isotropic filters can be obtained by a 2-D inverse Fourier transform or through the Hankel transform due to the symmetry of these filters with the orientation. Hence, the impulse functions are related to the Bessel functions. The discrete analog of the Gaussian kernel derives from the modified Bessel functions in [18]. In Fig. 7 the scaling function φ^n, the wavelet ψ^n, and the reconstruction wavelet χ^n are shown when $n = 4$. We see from (53) and (54) ψ^n are actually the good approximations of the Mexican hat or LoG wavelet.

For this type of wavelet transform, we can still derive filter bank algorithms for the decomposition and reconstruction as in the 1-D case. Defining the smoothing operation $S_{2^j}f$ and wavelet transform $W_{2^j}f$ as the 2-D convolutions of images with the scaling function (53) and LoG-like wavelets (54), the recursive decomposition formula reads,

$$\begin{cases} S_{2^j}f = S_{2^{j-1}}f * h_{\uparrow 2^{j-1}} \\ W_{2^j}f = S_{2^{j-1}}f * g_{\uparrow 2^{j-1}}, \qquad j = 1, 2\cdots J. \end{cases} \tag{56}$$

In the decomposition two components are obtained at each scale and the decomposition is implemented through the convolution with the 2-D nonseparable filter masks H and G in the time domain.

Through (50) the reconstruction formula is given by

$$\begin{aligned} S_{2^{j-1}}f = S_{2^j}f * h_{\uparrow 2^{j-1}} + W_{2^j}f * \tilde{g}_{\uparrow 2^{j-1}}, \\ j = J, J-1\cdots 1 \end{aligned} \tag{57}$$

where the transfer functions H, G, $\tilde{G}$ of the 2-D filters h, g, $\tilde{g}$ are governed by the condition (50) in the polar coordinates. Through such a condition it is easy to show using the same arguments as in the 1-D case that an image $f \in L^2(\mathbb{R}^2)$ can be represented in the continuous form by its isotropic components $\{W_{2^j}f\}_{j\in\mathbb{Z}}$ as

$$f(x, y) = \sum_{j=-\infty}^{\infty} W_{2^j}f * \chi_{2^j}^n(x, y), \quad (x, y) \in \mathbb{R}^2 \tag{58}$$

where $\chi_{2^j}^n$ is the reconstruction wavelet defined by (55).

In Fig. 6, the decomposition and reconstruction of a simulated image using the above formulae at several scales are displayed. The image is decomposed into two parts at each scale, one is the smoothed part and the other is the wavelet detail part. And the image can be synthesized from these two parts at multiple scales.

We find that when $n = 3$ the above designed filters are similar to those designed by Croft and Robinson [32] where they have used them for edge based image coding.

V. Image Representation by Multiscale and Multidirectional Derivative Components

A. Motivation

Oriented filters play a very important role in many vision tasks [30], [33], [34], such as the texture analysis, edge detection, motion analysis, image enhancement and so on. For example, Daugman [33] has applied 2-D Gabor bases to stress the importance of image orientation analysis. In this section, we would like to design multiscale filters with the orientation tunings such that the images can be synthesized from these multiscale and multidirectional bases.

Let us recall that in Section IV-A, in order to make the images to be synthesized from their vertical, horizontal and diagonal components, the designed transfer filter should satisfy the condition (45). We rewrite this condition as

$$\begin{aligned} H^2(\omega_x)H^2(\omega_y) + G_1(\omega_x)U_1(\omega_y) + G_2(\omega_y)U_2(\omega_x) \\ + G_3(\omega_x, \omega_y)U_3(\omega_x, \omega_y) = 1 \end{aligned} \tag{59}$$

where

$$\begin{aligned} G_1(\omega_x) &= G^{(2)}(\omega_x)\tilde{G}^{(2)}(\omega_x), \\ G_2(\omega_y) &= G^{(2)}(\omega_y)\tilde{G}^{(2)}(\omega_y), \\ G_3(\omega_x, \omega_y) &= G^{(1)}(\omega_x)G^{(1)}(\omega_y), \\ U_1(\omega_y) &= U(\omega_y), \\ U_2(\omega_x) &= U(\omega_x), \\ U_3(\omega_x, \omega_y) &= \tilde{G}^{(1)}(\omega_x)\tilde{G}^{(1)}(\omega_y). \end{aligned} \tag{60}$$

In other words, in order to do the directional decomposition and synthesis this identity has to be satisfied.

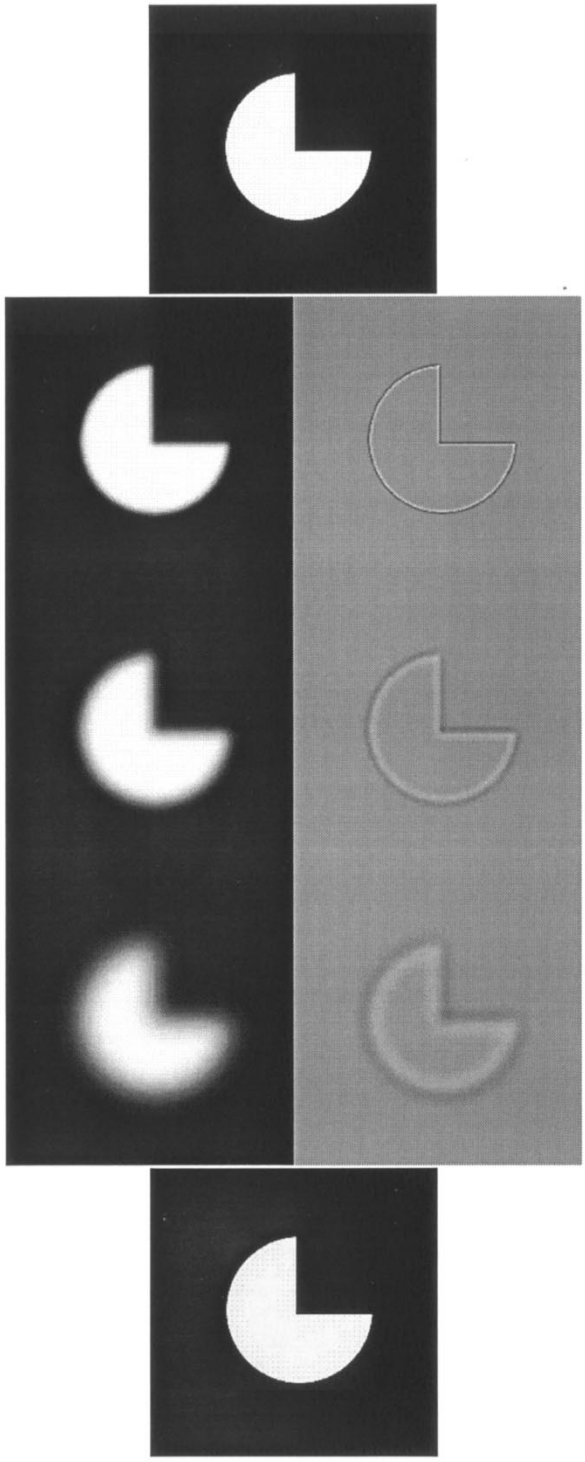

Fig. 6. Multiscale isotropic decompositions using filters shown in Fig. 7. At the top row is the simulated image and at the bottom row is the reconstructed image. Between them are the smoothing parts and the LoG-like components at dyadic scales 1, 2, and 4, respectively. The peanut-shaped homogeneous region appears due to the isotropic diffusion.

In this section, our purpose is to generalize the above case which decomposes an image along three orientations to a more general one. In other words, we will provide an alternative approach to decompose an image into dyadic scale derivative components with different orientation tunings. A more general perfect reconstruction condition than (59) for directional decomposition is presented in the design.

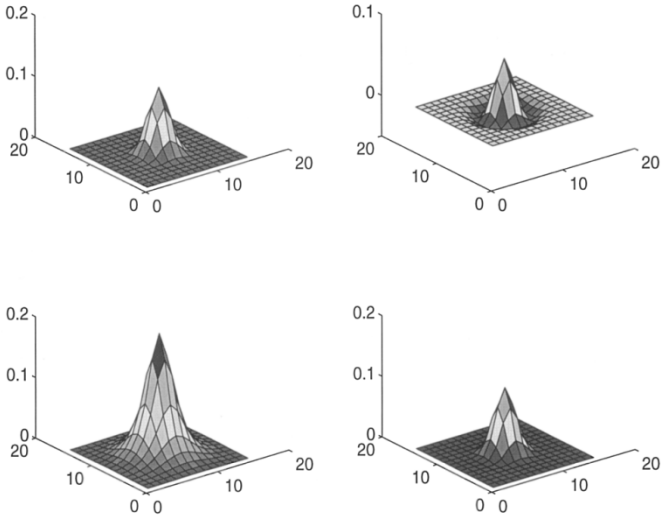

Fig. 7. Isotropic decomposition and reconstruction filters. Upper left: the scaling function (the radial B-spline of order four) for decomposition; upper right: the LoG-like wavelet function for decomposition; lower left: the wavelet function for reconstruction; lower right: the smoothing function for reconstruction, the same as in the upper left.

B. Design of Multiscale and Multidirectional Filters

Suppose the decomposition and synthesis filters are separable in the polar coordinates. That is, they can be written as the product of a radial function and angular function

$$\hat{V}(\omega_x, \omega_y) = U(r)A(\theta)$$

where r and θ are the polar coordinates of the frequency domain. A shift of $A(\theta)$ with respect to its argument corresponds to rotation of the 2-D basis function $\hat{V}(\omega_x, \omega_y)$. In the following design, the images are subdivided into a collection of subbands localized in both scales and orientations. The multiscale features are reflected by a recursive system guaranteed by (50) as in the Laplacian operator case. The oriented components are constrained by the following *generalized Pythagorean theorem*.

Theorem 1: The following generalized Pythagorean formula holds

$$\sum_{k=0}^{n-1} \cos^{2m}\left(\theta - \frac{k}{n}\pi\right) = \frac{(2m-1)!!}{(2m)!!}\, n, \quad (1 \le m \le n-1) \tag{61}$$

where $(2m)!! := (2m)\cdot(2m-2)\cdots 4\cdot 2$, $(2m-1)!! := (2m-1)\cdot(2m-3)\cdots 5\cdot 3\cdot 1$. The proof is left in the Appendix B. If $n = 2, m = 1$, it becomes the following form of the usual Pythagorean theorem

$$\cos^2\theta + \cos^2\left(\theta - \frac{\pi}{2}\right) = 1.$$

So we call (61) the generalized Pythagorean theorem. This identity can be useful in many other occasions, since it

indicates that a radial vector $f(r)$ can be synthesized from a finite number of directional components of its projections along equally spaced angles. In detail

$$f(r) = \sum_{k=0}^{n-1} (f(r) A_k(\theta)) \cdot \overline{A}_k(\theta) \tag{62}$$

where

$$A_k(\theta) = j \sqrt{\frac{(2m)!!}{(2m-1)!!n}} \cos^m \left(\theta - \frac{k}{n}\pi\right), \quad (0 \le k \le n-1) \tag{63}$$

where the n angular components are distributed over a circle. This is quite similar to the back-projection theorem arising in tomography when reconstructing a scalar field from its Radon transform along the continuous angles.

Now we can present the design principle and procedure in three steps.

1) Design the radial filter $H(r)$, $G(r)$, $\tilde{G}(r)$ as (51) and (52) as in the Laplacian case such that they satisfy the following perfect reconstruction condition

$$H^2(r) + G(r)\tilde{G}(r) = 1. \tag{64}$$

2) Multiply the radial decomposition filter $G(r)$ by the angular response functions $A_k(\theta)$ to obtain the oriented filters for decomposition

$$G_k(r, \theta) = G(r) A_k(\theta) \quad (0 \le k \le n-1) \tag{65}$$

where $A_k(\theta)$ is taken as in (63). Similarly, the oriented reconstruction filter can be obtained by

$$\tilde{G}_k(r, \theta) = \tilde{G}(r) \overline{A}_k(\theta) \quad (0 \le k \le n-1). \tag{66}$$

3) Perform the 2-D inverse Fourier transform of G_k, $\tilde{G}_k$ to obtain the impulse responses g_k, $\tilde{g}_k$ in the time domain.

Once we get the decomposition and reconstruction filters G_k, $\tilde{G}_k$, the n oriented wavelet functions for decomposition and reconstruction can be defined as

$$\hat{\psi}^k(2\omega_x, 2\omega_y) = G_k(r, \theta)\hat{\varphi}(r) \quad (0 \le k \le n-1) \tag{67}$$

$$\hat{\chi}^k(2\omega_x, 2\omega_y) = \tilde{G}_k(r, \theta)\hat{\varphi}(r) \quad (0 \le k \le n-1) \tag{68}$$

where the scaling function $\varphi(r)$ is given by the *nth-order radial B-spline* (53) in the polar coordinates. One can see that the above defined wavelets are obtained from the Mexican-like wavelet, but tuned to different orientations. In the above design, the angular part can be replaced with its absolute value $|A_k(\theta)|$, then the designed decomposition filters are angularly even-symmetric. This type of filters can be called filters with even phases, while the above designed filters are called filters with odd phases. This quadrature pair of filters differing in phase by $\pi/2$ can be used to extract different types of edges of images. The role of this pair of filters can be very similar to the complex Gabor wavelets [11], [33], [34]; nevertheless, using these filters computational efficiency can be obtained.

Having computed these multiscale oriented filters, we can perform the dyadic multidirectional wavelet decompositions $\{W_{2^j}^k f = f * \psi_{2^j}^k\}_{1 \le j \le J}^{0 \le k \le n-1}$ using the following recursive algorithm:

$$\begin{cases} S_{2^j} f = S_{2^{j-1}} f * [h]_{\uparrow 2^{j-1}} \\ W_{2^j}^k f = S_{2^{j-1}} f * [g_k]_{\uparrow 2^{j-1}} \qquad 0 \le k \le n-1, \end{cases} \tag{69}$$

where h is the 2-D radial smoothing filter mask in the time domain and g_k is the wavelet decomposition filter mask. The different orientations are indexed by k.

According to the above design procedure, it is easy to verify that the following perfect reconstruction condition holds:

$$\sum_{k=0}^{n-1} G_k(r, \theta)\tilde{G}_k(r, \theta) + H^2(r) = 1. \tag{70}$$

Then the reconstruction formula is given as

$$S_{2^{j-1}} f = S_{2^j} f * [\overline{h}]_{2^{j-1}} + \sum_{k=0}^{n-1} W_{2^j}^k f * [\tilde{g}_k]_{2^{j-1}}. \tag{71}$$

Furthermore, the following relation can be easily inferred

$$\sum_{k=0}^{n-1} \sum_{j=-\infty}^{\infty} G_k(2^j r, \theta)\tilde{G}_k(2^j r, \theta) = 1. \tag{72}$$

Hence, an image $f \in L^2(\mathbb{R}^2)$ can be represented in the continuous form from its multiscale and multidirectional components $\{W_{2^j}^k\}_{j \in \mathbb{Z}}^{0 \le k \le n-1}$ as

$$f(x, y) = \sum_{k=0}^{n-1} \sum_{j=-\infty}^{\infty} (W_{2^j}^k f * \chi_{2^j}^k)(x, y), \quad (x, y) \in \mathbb{R}^2. \tag{73}$$

It indicates that an image can be decomposed as the linear weighted sum of the oriented basis functions $\chi_{2^j}^k(x, y)$ at dyadic scales. The weights $W_{2^j}^k f$ reflect the edge information of images at both scales and orientations.

As an example, take $n = 4$, $m = 3$, and then the angular components in this case are

$$A_k(\theta) = j \frac{2}{\sqrt{5}} \cos^3 \left(\theta - \frac{k}{4}\pi\right) \quad (k = 0, 1, 2, 3).$$

According to (65), we obtain the decomposition filters G_k $(k = 0, 1, 2, 3)$ tuned to 0°, 45°, 90°, 135°, whose impulse responses in the time domain are shown in Fig. 8.

Fig. 9 are the decompositions and reconstruction of a texture image, which demonstrates the orientation information along four directions. The role of this decomposition is similar to that of the compass operators [29]. However, using our algorithm the images can not only be decomposed into as many orientations as desired but also can be recovered from these oriented components distributed at the dyadic scales.

A scheme for multiscale derivative computation was described in [31]. The orientation tuning is constrained by the

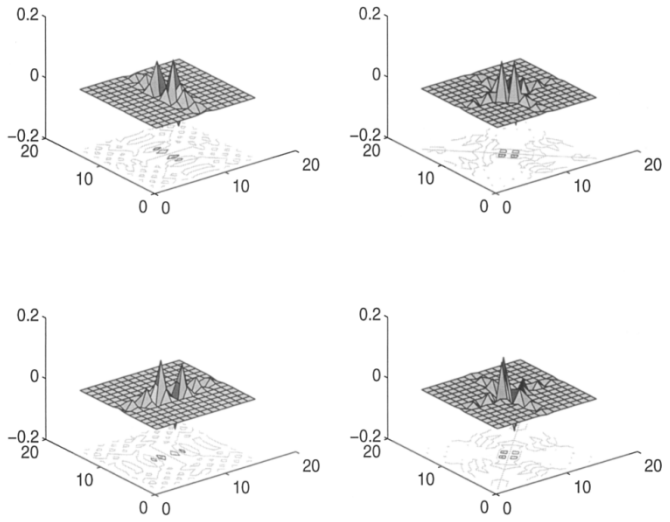

Fig. 8. Four oriented decomposition filters tuned to the orientations 0°, 45°, 90°, 135°, respectively. Here for illustration only four oriented filters are chosen. One can choose the filters to have as many orientational turnings as desired.

property of steerability [30] and the radial scaling components are constrained by a more tight recursive system. In comparison with this architecture, our proposed system is more redundant. The angular components are constrained by (61) and the radial components are required to satisfy (64). There is no down-sampling at each step of decompositions.

The Matlab code for generating the oriented wavelets can be obtained at http://wavelets. math.nus.edu.sg/~wyp/download_software/wavorien.m.

VI. Discussions

A. Relation with the Classical Gaussian Scale-Space Approaches

The well-known scaling theorem [36], [37], states that the Gaussian is the only kernel with the embedding property; it states that the number of zero-crossings does not increase as the scale becomes larger. For this reason, the classical scale-space is mainly based on the Gaussian kernel. One interesting point worth mentioning is the asymptotic behavior of the proposed spline wavelets as the order goes to infinity. The attractiveness of the spline wavelets would be their asymptotic convergence to the well-known edge detectors and their computational advantages. This establishes a rigorous link to Gaussian which has been shown to be optimal in minimizing information uncertainty, and has been used in a few famous edge detectors such as those of Marr–Hildreth [3] and Canny [5]. In the discrete implementation, the B-spline kernels also posses the scaling property like the Gaussian kernel [20]. The common properties shared by B-splines and Gaussian in a discrete setting can be understood in the framework of the total-positivity theory as memberships to *pólya* frequency classes [18]. Other properties such as the behaviors of edge patterns, the fingerprint theorem also holds in such case. For detailed discussions, refer to [20]. The most notable advantage of such representations in comparison with the classical multiscale approaches is their computational efficiency.

B. Relation with the Compact Wavelet Models

Multiscale differential operators such as the gradient operators and LoG operators have been widely used for image geometrical descriptions. However, it has not been clear whether the images can be recovered from these operators. Like the wavelets models [8], such representations can be made to be invertible, as shown in the paper. For discrete implementation, fast pyramid-like algorithms can also be derived. Different from the orthonormal wavelets models [8], [11], such representations are a little less compact and therefore retains some nice properties which are lack in orthonormal wavelet representations such as the *shift invariance*. For example, in denoising such type of wavelet representations has proved to be superior to the compact wavelet representations, which is subject to weaker visual artifacts [27].

C. On Visual Physiology and Psychophysics

A usual way to represent a signal by its differential operators is the Taylor polynomial expansion. Another used approach is the Hermite basis functions [40]. This paper proposes new mathematical methods. Since the power spectrum of the rth-order differential operator is proportional to $|\omega|^{2r}$ which corresponds to the spectrum of the fractal Brownian motion (fBm), the differential operations are usually regarded as the fBm process [41]. Therefore, in the stochastic sense the paper presents a family of models to synthesis a stochastic process from the fBm of certain orders diffused along the dyadic time scales in different forms, either isotropically or directionally. Also, it is not difficult to understand that the details of image information are carried on these wavelet representations since the fBm model is usually used to describe a variety of irregular structures like the textures. Multiscale spline approximations and differential operations are complementary techniques. One is aiming at extracting the deterministic components by diffusing the perturbation spatially while the other is to detect the stochastic components [41]. Moreover, neurophysiological studies by Young have provided evidence that there are receptive fields in the mammalian retina and visual cortex, whose measured response profiles can be very well modeled by Gaussian derivatives [18], [39]. Therefore, the proposed representation in the paper can be interpreted as one model for human visual modeling.

D. Comments on the Spline Approaches

The uniform B-splines are the only spline functions which are refinable and their shifts constitute a Riesz basis of $L^2(\mathbb{R})$ [22] or $l^2(\mathbb{Z})$ [15]. For this reason, we use B-splines for multiscale geometry analysis. In our opinion, the B-spline derivation is quite enlightening, as it elucidates the relationship between the edge detectors characterized by smoothed differentiation and the wavelets characterized by the two-scale difference equation. The explicit time domain expression for the FIR filters will be very useful in practice. Since these FIR filters are binomials, the wavelet algorithm can be realized only by *addition* operation. It should be noted that spline techniques have been widely used for fast implementation of

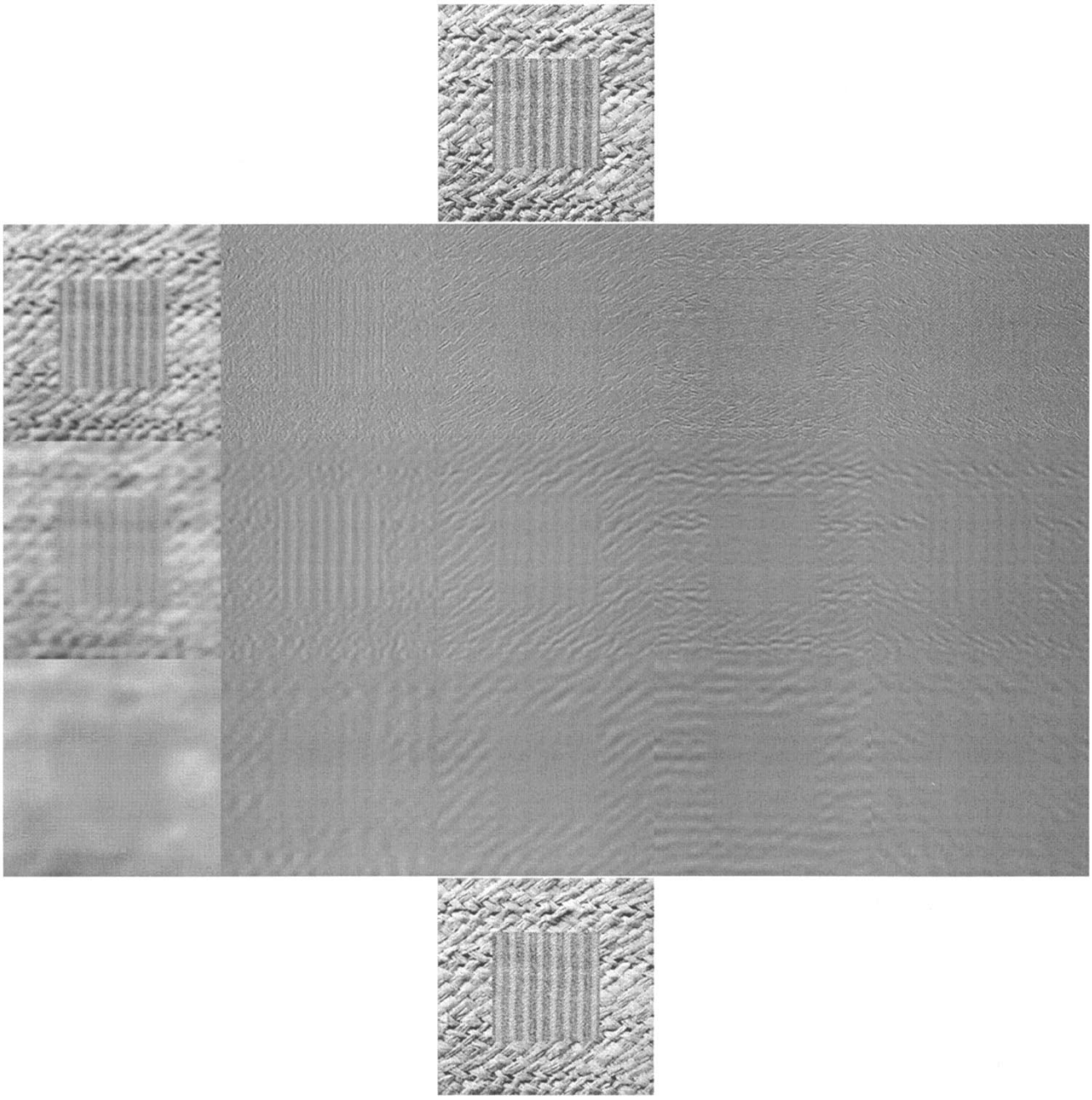

Fig. 9. Multiscale and multidirectional decompositions of a texture image using four oriented filters as shown in Fig. 8. At the top row is the simulated image and at the bottom row is the reconstructed image. Between them are the smoothing parts and the wavelet decompositions along four orientations at dyadic scales 1, 2, and 4, respectively. The filter size used was 7×7; a larger sized mask can achieve a high precision of reconstruction.

Gaussian scale-space filtering in computer vision even before the appearance of wavelets (for example, see [24] and [25]).

E. Comments on the Applications of Such Representations

Since the proposed representations have provided efficient and invertible representations of images, they can be very useful for geometry based applications. Some existing technology based on multiscale edge information can be found in [9], [28], and [32]. By making use of the multiscale geometric information offered by these representations, many other applications such as the stereo matching, edge based coding, filtering, enhancement, local orientation analysis can be done. We have used these representations for multiscale shape analysis [21]. We hope further applications can be exploited using the efficient algorithms developed in this paper.

VII. Conclusions

In this paper, efficient algorithms are designed for multiscale computations and representations of images using different types of differential operators such as the directional derivative and Laplacian operators. In particular, a general approach is

presented to represent images by their multiscale and multidirectional derivative components. For each type of wavelets, both the decomposition and reconstruction filter bank algorithms are derived for practical implementation. The proposed representations provide meaningful geometric information of images and hence can be useful for further applications.

APPENDIX A
RELATIONS BETWEEN B-SPLINES, BINOMIALS, AND THE FILTER BANKS

In Section III-A the B-spline wavelets (16) and (18) are selected as the first or second derivatives of B-splines. By this method, we arrive at the two-scale relations (11) and (21), where H is just the binomial filter, and G is the first or second order of difference operators. Conversely, if we define the filters H and G as binomials and difference operators respectively, the scaling function and the wavelets will be B-splines and their derivatives. Now we show their relations.

Consider the equivalent octave band nonsubsampled filter bank at level j

$$H^{(j)}(\omega) = \prod_{k=0}^{j-1} H(2^k\omega) \tag{74}$$

$$G^{(j)}(\omega) = G(2^{j-1}\omega)\prod_{k=0}^{j-1} H(2^k\omega). \tag{75}$$

In fact $H^{(j)}(\omega)$, $G^{(j)}(\omega)$ are the equivalent frequency impulses of the dyadic wavelet transform $W_{2^j}f$ and the smoothing approximation $S_{2^j}f$ at dyadic scale j directly from scale one.

$$\hat{S}_{2^j}f(\omega) = H^{(j)}(\omega)\hat{S}_{2^0}f(\omega)$$
$$\hat{W}_{2^j}f(\omega) = G^{(j)}(\omega)\hat{S}_{2^0}f(\omega).$$

Then, define the continuous functions $\varphi^{(j)}(x)$ and $\psi^{(j)}(x)$ by the finite impulse responses $h^{(j)}$, $g^{(j)}$ of $H^{(j)}$, $G^{(j)}$, i.e.,

$$\varphi^{(j)}(x) = 2^j h^{(j)}(n), \quad \frac{n}{2^j} \le x \le \frac{n+1}{2^j},$$
$$\psi^{(j)}(x) = 2^j g^{(j)}(n), \quad \frac{n}{2^j} \le x \le \frac{n+1}{2^j}$$

with $h^{(0)}$, $g^{(0)}$ defined as binomial and difference operators. Suppose the above definition converges in the $L^2(\mathbb{R})$ sense, then define φ and ψ by

$$\varphi(x) = \lim_{j\to\infty} \varphi^{(j)}(x), \quad x \in \mathbb{R}$$
$$\psi(x) = \lim_{j\to\infty} \psi^{(j)}(x), \quad x \in \mathbb{R}$$

it is not difficult to prove that these two functions are the B-splines (3) and B-spline wavelets (16) and (18). Since

$$\hat{\varphi}^{(j)}(\omega) = 2^j \sum_n h^{(j)}(n)\int_{n/2^j}^{(n+1)/2^j} e^{-i\omega x}dx$$
$$= \sum_n h^{(j)}(n)e^{-i(n\omega/2^j)}\frac{\sin\dfrac{\omega}{2^{j+1}}}{\dfrac{\omega}{2^{j+1}}}e^{-(\omega/2^{j+1})}$$
$$= H^{(j)}\Big(\frac{\omega}{2^j}\Big)\frac{\sin\dfrac{\omega}{2^{j+1}}}{\dfrac{\omega}{2^{j+1}}}e^{-(\omega/2^{j+1})}$$

and

$$H^{(j)}\Big(\frac{\omega}{2^j}\Big) = \prod_{k=0}^{j-1}\left(\cos 2^{k-j-1}\omega\right)^{n+1}$$
$$= \left(\frac{\sin 2^{-1}\omega}{2^{-1}\omega}\cdot\frac{\sin 2^{-j-1}\omega}{2^{-j-1}\omega}\right)^{n+1}$$

so

$$\hat{\varphi}^{\infty}(\omega) = \left(\frac{\sin 2^{-1}\omega}{2^{-1}\omega}\right)^{n+1}$$

i.e., $\varphi(x)$ is the B-spline of order n. The proof for $\psi(x)$ follows a similar procedure.

The above approach presents an intrinsic understanding of how the continuous B-splines can be obtained from the binomials. This is also closely related to the subdivision scheme [26].

APPENDIX B
PROOF OF THE GENERALIZED PYTHAGOREAN THEOREM

We give the proof using the mathematical induction. First, we will show that the formula holds for $m = 1$

$$\sum_{k=0}^{n-1}\cos^2\left(\theta - \frac{k}{n}\pi\right) = \frac{n}{2} \tag{76}$$

or equivalently

$$\sum_{k=0}^{n-1} e^{i(2\theta - 2(k/n)\pi)} = 0$$

which is equivalent to the sum of unit vectors distributed over an unit circle on complex plane. From the principle of geometry, this actually holds since the center of gravity of a polygon lies in the origin. Suppose now if $m = t \in \mathbb{Z}$, the formula (61) holds. Let's show this is true for the case $m = t + 1$. For simplicity, denote

$$f(\theta, n, t) = \sum_{k=0}^{n-1}\cos^{2t}\left(\theta - \frac{k}{n}\pi\right).$$

Taking second order derivative with respect to θ, it's not difficult to verify that $f(\theta, n, t+1)$ satisfy the following second-order ordinary differential equation (ODE)

$$f''(\theta, n, t+1) + (2t+2)^2 f(\theta, n, t+1) - (2t+2)(2t+1)f(\theta, n, t) = 0.$$

Since $f(\theta, n, t)$ is a constant $((2t-1)!!/(2t)!!)n$, the solution of the above equation should be

$$f(\theta, n, t+1) = c_1\cos(2t+2)\theta + c_2\sin(2t+2)\theta + \frac{(2t+1)!!}{(2t+2)!!}n$$

where c_1, c_2 is the constant coefficient to be determined. Because $f(\theta, n, t+1)$ is an even function, then $c_2 = 0$. Moreover, $f(\theta, n, t+1)$ is periodic with $(2/n)\pi$, it follows that $c_1 = 0$. Therefore, the solution becomes

$$f(\theta, n, t+1) = \frac{(2t+1)!!}{(2t+2)!!}n.$$

This completes the proof by the mathematical induction.

REFERENCES

[1] P. J. Burt and E. Adelson, "The Laplacian pyramid as a compact image code," *IEEE Trans. Commun.*, vol. 31, pp. 482–540, 1983.

[2] P. J. Burt, "Fast hierarchical correlations with Gaussian-like kernels," *Comput. Vis., Graph., Image Process.*, vol. 16, pp. 20–21, 1981.

[3] D. Marr and E. Hildreth, "Theory of edge detection," in *Proc. R. Soc. Lond. B*, vol. 207, pp. 187–217, 1980.

[4] A. P. Witkin, "Scale-space filtering," in *Proc. 7th Joint. Conf. Artif. Intell.*, Karlsruhe, Germany, 1983, pp. 1019–1023.

[5] J. Canny, "A computational approach to edge detection," *IEEE Trans. Pattern Anal. Machine Intell..*, vol. PAMI-8, pp. 679–698, 1986.

[6] M. Barlaud, T. Gaidon, P. Mathieu and J. C. Feauveau, "Edge detection using recursive biorthogonal wavelet transform," in *Proc. ICASSP'91*, pp. 2553–2556.

[7] J. L. Crowley and R. M. Stern, "Fast computation of the difference of low pass transforms," *IEEE Trans. Trans. Pattern Anal. Machine Intell.*, vol. PAMI-6, pp. 212–222, 1984.

[8] S. Mallat, "A theory for multiresolution signal decomposition: The wavelet representation," *IEEE Trans. Pattern Anal. Machine Intell.*, vol. 11, pp. 674–693, July 1989.

[9] S. Mallat and S. Zhong, "Characterization of signals from multiscale edges," *IEEE Trans. Pattern Anal. Machine Intell.*, vol. 14, pp. 710–732, July 1992.

[10] S. Mallat and W. L. Huang, "Singularity detection and processing with wavelets," *IEEE Trans. Inform. Theory*, vol. 32, pp. 617–643, Mar. 1992.

[11] S. Mallat, *A Wavelet Tour of Signal Processing.* New York: Academic, 1998, ch. VI.

[12] V. Torre and T. A. Poggio, "On edge detection," *IEEE Trans. Pattern Anal. Machine Intell.*, vol. PAMI-8, pp. 147–163, 1986.

[13] M. Unser, A. Aldroubi, and M. Eden, "B-spline signal processing: Parts 1 and 2," *IEEE Trans. Signal Processing*, vol. 41, pp. 821–847, 1993.

[14] ——, "On the asymptotic convergence of B-spline wavelets to Gabor functions," *IEEE Trans. Inform. Theory*, vol. 38, pp. 864–872, Mar. 1992.

[15] A. Aldroubi, M. Eden, and M. Unser, "Discrete spline filters for multiresolutions and wavelets of l_2," *SIAM J. Math. Anal.*, vol. 25, pp. 1412–1432, Sept. 1994.

[16] M. Unser, A. Aldroubi, and M. Eden, "Fast B-spline algorithms for continuous image representation and interpolation," *IEEE Trans. Pattern Anal. Machine Intell.*, vol. 13, pp. 277–285, Mar. 1991.

[17] T. Lindeberg, "Discrete derivative approximations with scale-space properties: A basis for low-level feature detection," *J. Math. Imag. Vis.*, vol. 3, pp. 349–376, 1993.

[18] ——, *Scale-Space Theory in Computer Vision.* Boston, MA: Kluwer, 1994.

[19] K. Toraichi, M. Kamada, S. Itahashi, and R. Mori, "Window functions represented by B-spline functions," *IEEE Trans. Acoust., Speech, Signal Processing*, vol. 37, pp. 145–147, 1989.

[20] Yu-Ping Wang and S. L. Lee, "Scale-space derived from B-splines," *IEEE Trans. Pattern Anal. Machine Intell.*, vol. 20, pp. 1040–1055, Oct., 1998.

[21] Yu-Ping Wang, S. L. Lee, and K. Toraichi, "Multiscale curvature based shape representation using B-spline wavelets," *IEEE Trans. Image Processing*, vol. 8, pp. 1586–1592, Nov. 1999.

[22] W. Lawton, S. L. Lee, and Z. Shen, "Characterization of compactly supported refinable splines," *Adv. Comput. Math.*, vol. 3, pp. 137–145, 1995.

[23] R. Deriche, "Using Canny's criteria to derive a recursively implemented optimal edge detector," *Int. J. Comput. Vis.*, vol. 1, pp. 167–187, 1987.

[24] M. Wells, "Efficient synthesis of Gaussian filters by cascaded uniform filters," *IEEE Trans.Pattern Anal. Machine Intell.*, vol. PAMI-8, pp. 234–239, 1986.

[25] L. A. Ferrari, P. V. Sankar, S. Shinnaka, and J. Sklansky, "Recursive algorithms for implementing digital image filters," *IEEE Trans. Trans. Pattern Anal. Machine Intell.*, vol. PAMI-9, pp. 461–466, 1987.

[26] N. Dyn and D. Levin, *The Subdivision Experience, Wavelets, Images and Surface Fitting*, P. J. Laurent *et al.*, Eds. Wellesley, MA: A. K. Peters, 1994, pp. 229–244.

[27] R. R. Coifman and D. L. Donoho, "Translation invariant denosing," *Wavelets and Statistics*, A. Antoniadis and G. Oppenheim, Eds. Berlin, Germany: Springer-Verlag, 1995, p. 125.

[28] Y. Xu, B. Weaver, D. M. Healy, and J. Lu, "Wavelet domain filters: A spatial selective noise filtration technique," *IEEE Trans. Image Processing*, vol. 3, pp. 747–757, Nov. 1994.

[29] A. K. Jain, *Fundamentals of Digital Image Processing.* Englewood Cliffs, NJ: Prentice-Hall, 1989.

[30] W. T. Freeman and E. H. Adelson, "The design and use of steerable filters," *IEEE Trans. Pattern Anal. Machine Intell.*, vol.13, pp. 891–906, Sept. 1991.

[31] E. P. Simoncelli and W. T. Freeman, "The steerable pyramid: A flexible architechure for multiscale derivative computation," in *Proc. 2nd IEEE Int. Conf. on Image Processing*, 1995, vol. III, pp. 444–447.

[32] L. H. Croft and J. A. Robinson, "Subband image coding using watershed and watercourse lines of the wavelet transform," *IEEE Trans. Image Processing*, vol. 3, pp. 759–771, 1994.

[33] J. G. Daugman, "Complete discrete 2-D Gabor transform by neural networks for image analysis and compression," *IEEE Trans. Acoust., Speech, Signal Processing*, vol. 36, pp. 107–114, 1988.

[34] A. Bovik, M. Clark, and W. Geisler, "Multichannel texure analysis using localized spatial filters," *IEEE Trans. Pattern Anal. Machine Intell*, vol. 12, pp. 55–73, 1990.

[35] A. L. Yuille and T. Poggio, "Fingerprints theorems for zero-crossings," *J. Opt. Soc. Amer. A*, vol. 2, pp. 683–692, 1985.

[36] ——, "Scaling theorems for zero-crossings," *IEEE Trans. Pattern Anal. Machine Intell.*, vol. PAMI-8, pp. 15–25, 1986.

[37] J. Babaud, A. P. Witkin, M. Baudin, and R. 0. Duda, "Uniqueness of Gaussian kernel for scale-space filtering," *IEEE Trans. Pattern Anal. Machine Intell.*, vol. PAMI-8, pp. 26–33, 1986.

[38] A. Rosenfeld and M. Thurston, "Edge and curve detection for visual scene analysis," *IEEE Trans. Comput.*, vol. C-20, pp. 562–569, 1971.

[39] R. A. Young, "The Gaussian derivative model for spatial vision: I. Retinal mechanisms," *Spatial Vis.*, vol. 2, pp. 273–293, 1987.

[40] J. B. Martens, "The Hermite transform-theory," *IEEE Trans. Acoust., Speech, Signal Processing*, vol. 38, pp. 1595–1606, 1990.

[41] R. Szeliski and D. Terzopoulis, "From splines to fractals," *Comput. Graph.*, vol. 23, pp. 51–60, 1989.

Yu-Ping Wang received the B.Sc. degree in applied mathematics in 1990 from Tianjin University, China, and the M.Sc. degree in computational mathematics and the Ph.D. degree in communication and electronic systems, both from Xi'an Jiaotong University, China, in 1996 and 1993, respectively.

He has been a Research Fellow with the Wavelets Strategic Research Programme, National University of Singapore, since 1996. In 1999, he joined the Washington University Medical Center, St. Louis, MO, where he works on medical image analysis. His current research interests include computer vision, signal analysis and various applications of wavelets, partial differential equations, fractals, and splines.